Remote Sensing of Environment 195 (2017) 218–229

Contents lists available at ScienceDirect

Remote Sensing of Environment

journal homepage: www.elsevier.com/locate/rse

Assessing the impact of emerging forest disease on wildfire using Landsat and KOMPSAT-2 data

Gang Chen [a,*], Yinan He [a], Angela De Santis [b], Guosheng Li [c], Richard Cobb [d], Ross K. Meentemeyer [e,f]

[a] Laboratory for Remote Sensing and Environmental Change (LRSEC), Department of Geography and Earth Sciences, University of North Carolina at Charlotte, 9201 University City Blvd, Charlotte, NC 28223, USA
[b] Centro Regional Fundación CEQUA, 21 de mayo 1690, Punta Arena, Chile
[c] Key Laboratory of Land Surface Pattern and Simulation, Institute of Geographic Sciences and Natural Resources, Chinese Academy of Sciences, 11A Datun Road, Beijing 100101, China
[d] Department of Plant Pathology, University of California, 1 Shields Ave, Davis, CA 95616, USA
[e] Center for Geospatial Analytics, North Carolina State University, 3120 Jordan Hall, Raleigh, NC 27695, USA
[f] Department of Forestry and Environmental Resources, North Carolina State University, 3120 Jordan Hall, Raleigh, NC 27695, USA

ARTICLE INFO

Article history:
Received 20 March 2016
Received in revised form 29 March 2017
Accepted 11 April 2017
Available online xxxx

Keywords:
Forest disease
Burn severity
Object-based filter
Landsat
KOMPSAT-2
Interacting disturbances

ABSTRACT

Environmental disturbance regimes are more frequently being altered by historically novel events and disturbance interactions, which may trigger reorganizations of new ecosystem states and processes. Here we examine synergies between emerging forest disease and wildfire to determine whether disease outbreak changes environmental drivers of burn severity using sudden oak death and the basin complex fire in California as a case study of novel disturbance interaction. We mapped the spatial distribution of sudden oak death tree mortality using a new object-based filter with 1.0 m resolution KOMPSAT-2 images. We integrated these data with a physical simulation model of burn severity informed by post-fire Landsat data. Model performance varied across stages of disease establishment (early, middle and late) with stronger relationships occurring during later stages of disease progression. Multiscale statistical analysis of environmental drivers of burn severity in diseased compared to healthy forests showed that sudden oak death tree mortality altered relationships between burn severity and the biophysical environment. Specifically, compared to the healthy forests, those affected by disease exhibited higher landscape heterogeneity at smaller spatial scales (e.g., 25 and 50 m), which has been associated with decreased burn severity in the literature. Our results showed the opposite pattern. That is, a disease-affected landscape comprising less connected patches and higher patch shape complexity was more likely to experience greater burn severity. This suggests that disease-caused increases in surface fuels may have reduced the landscape's resistance to fire and in turn increased burn severity in forest patches neighboring disease-impacted forests.

1. Introduction

Forest ecosystems have been increasingly affected by a variety of environmental tree-mortality disturbances (Asner, 2013; Johnstone et al., 2016). Wildfires and invasive species, including disease-causing pathogens and insects, are important drivers of tree mortality in key forest biomes worldwide (Boyd et al., 2013; Stephens et al., 2013). Although each disturbance type has been studied from a variety of perspectives, recent studies discovered that wildfire dynamics can be influenced by invasion of exotic forest pathogens and insects (Metz et al., 2011; Harvey et al., 2013). This introduces a critical question for forest managers and ecologists: does pre-fire disease or insect driven mortality alter wildfire dynamics and the associated ecological impacts (Hicke et al., 2012; Metz et al., 2013)?

The relevance of this question is self-evident from the spatial scale and frequency of these mortality events, yet the current state of knowledge lacks a synthetic framework of how forest diseases/insects and wildfires interact. Previous studies have attempted to analyze the direct relationship between disease/insect occurrence and burn severity at the stand scale. These efforts have shown specific results that could be seen as inconsistent: some researchers discovered weak correlations between outbreak and fire impacts while others reported evidence that this relationship could be enhanced or diminished (e.g., Metz et al., 2011; Simard et al., 2011; Hicke et al., 2012; Jolly et al., 2012; Harvey et al., 2013). However, in forests without active insect or disease outbreaks, a large body of research employing physical and empirical fire models has shown a strong tie between fire behavior and several controlling environmental factors, such as landscape configuration, and

* Corresponding author.
E-mail address: gang.chen@uncc.edu (G. Chen).

http://dx.doi.org/10.1016/j.rse.2017.04.005
0034-4257/

topography (Turner and Romme, 1994; Lloret et al., 2002; Balbi et al., 2009; Lee et al., 2009). This suggests that inconsistent results between disease/insect impacts and burn severity could be a reflection of complex environmental factors that mask or obscure outbreak-fire interactions. The introduction of diseases or insects are known to alter the physical and biological factors that affect wildfire dynamics such as intensity and ecological impacts by increasing surface fuel, and restructuring forest canopy. However, tree mortality also increases landscape heterogeneity by decreasing canopy continuity and altering species composition. These ecological effects are especially prominent for generalist pathogens and insects that cause selective tree mortality within or among landscape elements (Meentemeyer et al., 2008; Cobb et al., 2012). Compared to a homogenous surface structure, higher heterogeneity could enhance the fire-resistance of a landscape (Lee et al., 2009). To inform effective fire modeling and management in outbreak-impacted forests, it is vital to understand how disease or insect outbreak may alter landscape structure that is known to influence fire. This kind of investigation is a potentially valuable complement to the stand-level investigations that currently underpin our knowledge of outbreak-fire interactions and, ideally, would resolve inconsistencies among studies at this spatial scale. Specifically, whether and how does a disease or insect epidemic change the environmental factors affecting burn severity at the landscape scale? Understanding these dynamics is likely to positively contribute to the growing exploration of connections between insect- or disease-induced tree mortality and wildfire impacts (Metz et al., 2013; Simard et al., 2011).

Landscape heterogeneity has long been recognized to be scale-dependent in ecology and remote sensing (Levin, 1992; Wu, 2004). Spatial scale is a crucial factor for assessing the effect of disease or insect epidemic on burn severity. For example, the plant disease sudden oak death (SOD) has a non-random, highly-localized distribution at the landscape scale (Davidson et al., 2005). At the extent of a small field plot or fine grain resolution (e.g., 25 m), infestation may be uniform and homogenous causing damage on all or most trees (Cobb et al., 2012). At this spatial extent, disease has been shown to increase burn severity and fire-associated mortality under some disease conditions (Metz et al., 2013). However, at a larger scale or coarser grain (e.g., 400 m), a plot is more likely to contain a less-uniform distribution of tree damage or mortality. This is especially true in forests with heterogeneous species distributions and can complicate inference when plots are nested and have different levels of resolution. While post-fire landscape structure was confirmed to be affected by fires (e.g., causing short-term spatial homogenization; Chuvieco, 1999), a particularly important concern yet to be well addressed is how burn severity might be associated with pre-fire landscape spatial patterns emerging from plant community or mortality distribution.

Understanding these relationships requires spatially explicit mapping of forest damage by disease/insect and fire disturbances (respectively); remote sensing offers a feasible solution to this important problem. Over the past decade, research efforts have increasingly focused on extracting remotely sensed indicators of tree damage or distinct symptoms (i.e., altered spectral and spatial characteristics) as opposed to their healthy counterparts (e.g., Kelly and Meentemeyer, 2002; Lentile et al., 2006; Wulder et al., 2006; Keeley, 2009). For example, high-spatial resolution (h-res) imagery (typically finer than 5 m) can achieve a measurement scale and accuracy similar to field surveys (Wulder et al., 2006; Meentemeyer et al., 2008). Meanwhile, burn severity mapping has benefited from the use of a range of satellite and airborne sensors (e.g., MODIS, Landsat and AVIRIS) that can capture the unique spectral radiance from active fires or post-fire deposits of char, shoot, and ash (see Lentile et al., 2006; Keeley, 2009). Specifically, remote sensing of burn severity has two groups of models: physically based versus empirical (De Santis and Chuvieco, 2007). Empirical models are easy to implement applying statistical functions or thresholding to directly link burn severity with spectral responses/indices [e.g., Normalized Burn Ratio (NBR), differenced NBR, NDVI, and differenced NDVI] (e.g., Xiao et al., 2002; Epting et al., 2005; van Wagtendonk et al., 2004; Key and Benson, 2005; Kokaly et al., 2007). However, their performance is typically dependent on specific sites. In contrast, physically based simulation models have proven to be effectively reducing variation in model performance across geographical regions (Roy et al., 2006; De Santis and Chuvieco, 2007). For example, De Santis et al. (2009) integrated two radiative transfer models of PROSPECT and GeoSail to simulate the spectra of burned materials in forests. Quintano et al. (2013) applied Multiple Endmember Spectral Mixture Analysis (MESMA), a classic spectral unmixing approach to decompose pixels into four components of unburned and low, moderate, and high levels of burn severity.

In 2008, basin complex fire occurred in the Big Sur ecoregion of California, where a landscape-level permanent plot network designed to study sudden oak death emergence and associated ecological impacts was established between 2006 and 2007. The happenstance of fire and disease overlap with extensive pre-fire field data provides an unprecedented opportunity to study the influence of disease-caused tree mortality on burn severity at different spatial scales. We ask two inter-related research questions: did the pre-fire outbreak of sudden oak death alter the environmental factors that control burn severity? What was the role of spatial scale in determining disease-fire interactions? To address these questions, we employed h-res KOMPSAT-2 and Landsat imagery to map forest damage caused by sudden oak death and the basin complex fire, respectively. We then developed statistical models to link burn severity and its controlling environmental factors comparing diseased and healthy forests across spatial scales.

2. Study area and data

2.1. Study area

The study area (36°16′N, 121°44′W) is located in the Big Sur ecoregion on the western flank of the Santa Lucia Mountains in California covering 28,383 ha (Fig. 1). It features a Mediterranean climate and a rugged landscape dissected by steep slopes and drainages with elevations ranging from sea level to 1571 m within 5 km of the coast (Meentemeyer et al., 2008). Landownership in Big Sur is dominated by state and federal governments, and local conservation organizations (85%; Meentemeyer et al., 2008). The region primarily includes mixed oak forests consisting of coast live oak, Shreve's oak, tanoak, bay laurel (*Umbellularia californica*), and madrone (*Arbutus menziesii*; Davis et al., 2010). Redwood (*Sequoia sempervirens*)-tanoak forests dominate wetter landscape positions including ridgetops near the ocean with high frequency occurrence of fog and canyon bottoms, also near the ocean (Davis et al., 2010). There are also small patches of mixed coniferous trees, primarily ponderosa pine (*Pinus ponderosa*), coulter pine (*P. coulteri*), and Santa Lucia Fir (*Abies bracteata*). Chaparral shrubland, annual grassland, and bare ground comprise the remainder (Davis et al., 2010).

Sudden oak death (SOD), an emergent forest disease caused by the non-native pathogen *Phytophthora ramorum*, has killed tens of thousands of trees - primarily coast live oak and tanoak - in the Big Sur area since the mid-1990s (Rizzo et al., 2005). The canopies of dead trees change dramatically from healthy green to brown within 2–8 years of infection (Cobb et al., 2012), which makes it possible to remotely detect the disease (Kelly and Meentemeyer, 2002). The spread of *P. ramorum* across the landscape has a patchy distribution, and local forest stands span a range of disease impacts and time since pathogen establishment (Metz et al., 2011). Most pathogen dispersal occurs on a small (1–15 m) spatial scale, but long-distance (1–2 km) dispersal occurs during high precipitation storm systems with sustained winds (Meentemeyer et al., 2011). In June 2008, the basin complex fire was ignited by a dry lightning storm, which occurred following several months of low precipitation, and warm temperatures that reduced fuel moisture levels. The basin fire burned virtually all forest types

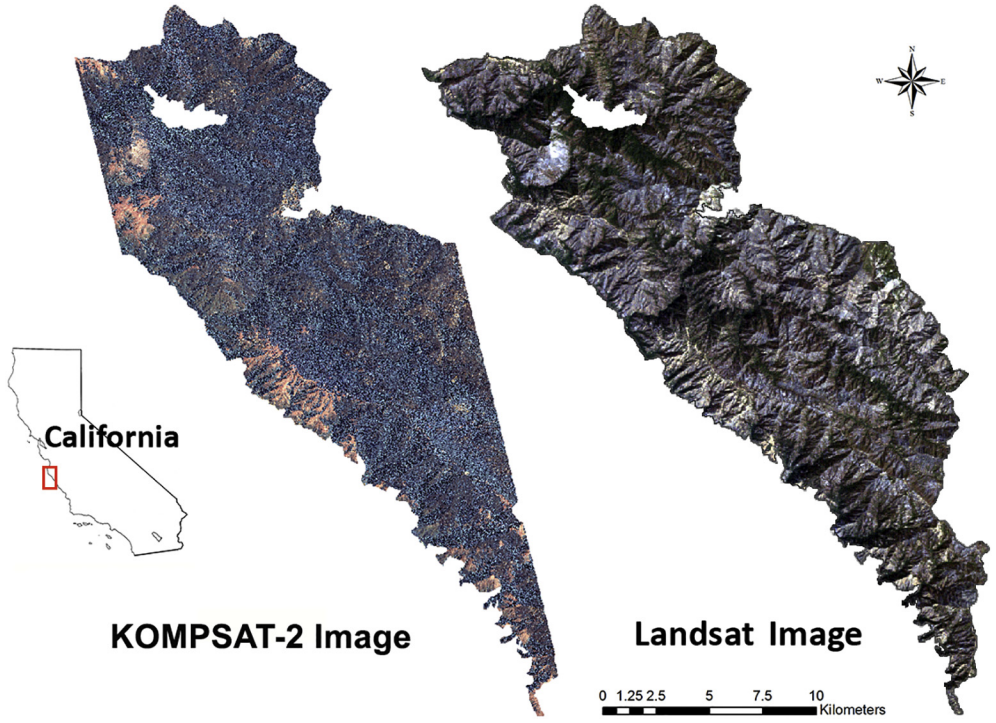

Fig. 1. Study area located in the Big Sur ecoregion on the western flank of the Santa Lucia Mountains in California, and represented by two remote sensing color composites, including KOMPSAT-2 bands 4 (red), 1 (green), and 2 (blue), and Landsat TM bands 3 (red), 2 (green), and 1 (blue). (For interpretation of the references to color in this figure legend, the reader is referred to the web version of this article.)

within Big Sur including those with *P. ramorum* hosts that we focus on here. In total, the basin fire affected a total of over 95,000 ha (USDA Forest Service, 2008).

2.2. Field data

A total of 61 circular plots (500 m^2 each) were burned during the basin fire; these plots were established as part of the previously noted long-term monitoring network (280 plots) designed to understand pathogen spread factors and measure *P. ramorum* caused forest mortality rates and ecological impacts (Meentemeyer et al., 2008; Metz et al., 2012). A full census of vegetation was conducted in each plot: all stems >1 cm diameter at breast height (dbh) were mapped, measured, and assessed for disease symptoms; all understory plants were identified to species and rated for cover; canopy cover was estimated with by averaging four densitometer measurements taken at ~1 m height at four cardinal directions at plot center. The locations of plots were randomly selected within mixed evergreen forests (often oak-dominated). One year prior to the basin complex fire, 42 of these plots were confirmed to have been invaded by *P. ramorum* through direct pathogen isolation; 19 of these plots had no disease symptoms and the pathogen was never isolated from any trees within or nearby (see Metz et al., 2011). Following the containment of the fire, these plots were revisited between September and October of 2008 to assess burn severity in five forest strata: (1) substrate layer, measured as changes to coarse woody debris, soil, duff, and leaf litter; (2) herb layer, changes or responses of vegetation <1 m; (3) shrub layer, changes of vegetation higher than 1 m but <5 m; (4) intermediate-sized tree layer, any trees higher than 5 m but standing under the dominant trees (intermediate canopy position); and (5) dominant tree layer (Metz et al., 2011). To quantify the plot-level burn severity, the GeoCBI field protocol (De Santis and Chuvieco, 2009) was adopted, where a rating from 0.0 to 3.0 represents the degree of burn severity from low to high. We employed GeoCBI rather than the classic Composite Burn Index (CBI, Key and Benson, 2005), because it takes into account the weighting factor Fractional Cover (FCOV) to describe burn severity. More importantly, GeoCBI considers the fractional cover of different vegetation strata, which better reflects the spectral mixture of those components from remote sensing with a 'top-down' view. This approach has been shown to be suitable for remote-detection based study (De Santis and Chuvieco, 2009). We found our densitometer estimate of canopy cover was preferable over total basal area or stem density estimated from plot-based vegetation surveys as this measure 1) directly estimated cover of dead trees and 2) heterogeneous canopy cover within plots. Therefore, FCOV per forest stratum was calculated by multiplying the pre-fire canopy cover and the post-fire proportion of green vegetation.

2.3. Topographic data

The regional topographic condition was represented by a 30 m resolution DEM (digital elevation model), derived from the Advanced Spaceborne Thermal Emission and Reflection Radiometer (ASTER) Global Digital Elevation Model Version 2 (GDEM V2) (ASTER GDEM Validation Team, 2011). Slope and aspect were further generated from the DEM, with the consideration that these two factors alter microclimate (e.g., wind speed and solar insolation) and therefore may have contributed to the variation in burn severity (Rogan and Franklin, 2001). Another topography-related factor Topographic Moisture Index (TMI) was also used to assess the potential impact of surface wetness on burn severity. The TMI variable was calculated from the DEM-generated parameters including upstream contributing area a and slope b (Eq. (1); Beven and Kirkby, 1979) according to:

$$\mathrm{TMI} = \ln(a/\tan b) \quad (1)$$

2.4. KOMPSAT-2 imagery

Five scenes of h-res KOMPSAT-2 satellite data were acquired on June 23, 2007 for the purpose of detecting *P. ramorum* caused tree mortality which can be non-random and patchy at fine spatial scales (Meentemeyer et al., 2008). All the images were ordered at the level

of 1G, where geometric and radiometric corrections were completed by the vendor. Each image scene included four 4 m multispectral bands [i.e., band 1 (520–600 nm, green), band 2 (450–520 nm, blue), band 3 (760–900 nm, near-infrared), and band 4 (630–690 nm, red)] and one 1 m panchromatic band (500–900 nm), with a radiometric resolution of 10 bits. To exploit both the spatial and multispectral content of the imagery (i.e., obtaining 1 m multispectral data), a principal components spectral sharpening technique was used to fuse each scene of multispectral and panchromatic bands (Welch and Ahlers, 1987). This pan-sharpening method has proven effective in a forest environment using Quickbird imagery that has the similar spectral and spatial characteristics as the KOMPSAT-2 data (Chen et al., 2011). We mosaicked all the five scenes using the overlapped area from one image to balance the data range of its neighboring image, which was followed by the application of the dark object subtraction algorithm to derive surface reflectance (Chavez, 1996). The pre-processed KOMPSAT-2 mosaic is shown in Fig. 1, where only a small portion of the area was not covered within the fire boundary.

2.5. Landsat imagery

A Landsat-5 TM image scene covering the same study area (Path 43, Row 35) was acquired on September 2, 2008 from the USGS archive in L1T format (radiometrically, geometrically and topographically corrected) to represent post-fire forest conditions in the study area (Fig. 1). The image had solar zenith angle of 36.2°, and solar azimuth angle of 135.9°. Here, the image scene was a surface reflectance product delivered by USGS. While a new Landsat Collect 1 L1TP product was published by USGS (in September 2016) with a higher terrain precision to support time-series processing analysis (USGS, 2016), this single-date L1T image scene had sufficient location accuracy for the study.

3. Methods

3.1. Disease mapping

Previous studies have confirmed the feasibility of using 1 m resolution remotely sensed imagery to extract *P. ramorum* caused dead trees (Kelly and Meentemeyer, 2002; Liu et al., 2006), the pan-sharpened KOMPSAT-2 data were expected to contain sufficient spatial details for disease mapping in this study. At the high resolution, each dead tree crown or dead crown cluster was comprised of a group of connected pixels (i.e., image-object). Meentemeyer et al. (2008) mapped *P. ramorum* caused tree mortality in Big Sur and found Geographic Object-Based Image Analysis (GEOBIA) was suitable to extract and analyze these image-objects. Specifically, image segmentation was conducted on the KOMPSAT-2 mosaic in the eCognition Developer 8 environment (Trimble Navigation, Sunnyvale, California). Three parameters were defined, including scale (60), shape (0.5) and compactness (0.8). The value of 60 was chosen for the purpose of accurately extracting clusters of trees that were relatively small and homogenous, e.g., the majority of trees within image-objects were either dead or healthy. The large compactness value was chosen to generate compact tree objects that could also have relatively smooth boundaries (Chen et al., 2012a). We applied the classic nearest neighbor classifier in eCognition to categorize all the image-objects into four land-cover classes, including healthy forest, disease-impacted forest, bare ground, and grass/shrub. The inputs of classification comprised three groups of features calculated at the object level: spectral (mean), texture (standard deviation), and geometry (compactness, length/width ratio, roundness, and shape index) (Table 1). In total, 13 features were calculated (refer to Table 1 for detailed description of each feature). To increase processing efficiency while retaining the classification performance, we reduced the number of input features by following a rule suggested by eCognition that the combination of features produces the largest average minimum distance between the samples of different classes, while the addition of extra features only marginally contributes to the improvement of classification accuracy.

Table 1
Object-based input features used in disease mapping.[a]

Feature	Description
Spectral:	
▪ Mean	**Mean** includes average intensity values for each of the four spectral bands, and maximum differential values between the brightest and the darkest image bands.
Texture:	
▪ Standard deviation	**Standard deviation** is calculated for each of the four spectral bands.
Geometry:	
▪ Compactness ▪ Length/width ratio ▪ Roundness ▪ Shape index	**Compactness** is the product of the length and the width, divided by the number of pixels. **Length/width ratio** is calculated using the main line of an object. **Roundness** describes the similarity between an image object and an ellipse, and it is calculated by the difference of the enclosing ellipse and the enclosed ellipse. **Shape index** represents the smoothness of an object, and it is calculated from the length of the object divided by four times the square root of its area.

[a] See equations in the eCognition Developer Reference Book (Trimble, 2012).

The transitional zones (i.e., from dense forest to shrub/grass or bare ground) in our study area posed a major challenge to the accurate extraction of dead tree crowns. It was discovered in our preliminary tests that many image-objects within the transitional zones were misclassified as disease-impacted forest even if the trees were in fact healthy. This was mainly owing to the fact that each of these objects often contained mixed land-cover classes, such as sparsely distributed trees or small tree clusters, bare ground and shrubs/grass (Fig. 2). To address such issue, we developed an object-based filtering algorithm combining detailed forest spectral information inside image-objects and across their neighbors. Each object-based filter was defined to contain one center image-object and its immediately adjacent neighboring objects, which was followed by moving the filter across the classified image generated from the previous section. Specifically, (a) for any disease-impacted image-object having more than or equal to one bare ground or shrub/grass neighbor, it was considered to be located in the transitional zones for further analysis. (b) The internal spectral variation of the selected image-objects was used to examine whether the preliminary classification results were correct. We calculated the ratio of the number of tree-shadow pixels to the number of sunlit-healthy-crown pixels within each object. Please note that we did not focus on all the sunlit crowns. Instead, we only focused on the sunlit 'healthy' crowns. For a healthy forest, the ratio was normally lower than 1.0. This was a byproduct of tree clustering that cast shadows into canopy gaps and/or the boundaries of tree clusters. For remote sensing using the top-down view, it is difficult to capture the shadow beneath every sunlit canopy. For a disease-impacted forest, the ratio was normally higher than 1.0, because dead trees contained a small percentage of healthy crowns, while the shadows were from both healthy and dead crowns. The KOMPSAT-2 near-infrared band was manually interpreted to determine the thresholds for identifying tree shadows (reflectance value smaller than 0.28) and sunlit-healthy crowns (reflectance value larger than 0.56), based upon the knowledge that this band typically has the highest contrast in forest environments among the four analyzed multispectral bands (Chen et al., 2011). (c) The center image-object previously classified as disease-impacted was reassigned if its ratio analysis indicated healthy trees in the object. To simplify our analysis, we assigned one single class to each image-object through a simple majority rule, where the newly assigned class was consistent with the one having the largest coverage across the neighbors.

Calibration (training) and validation of the classification and filtering processes were conducted using the combination of field data, and image manual interpretation on the KOMPSAT-2 and Google Earth

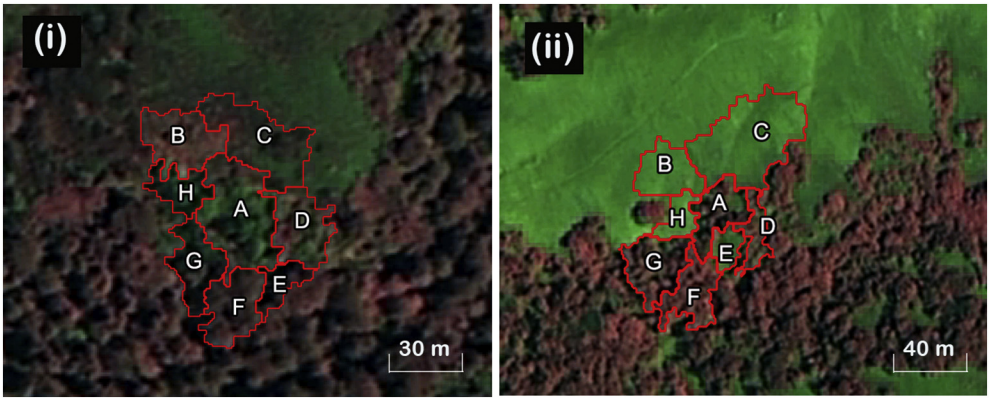

Fig. 2. (i) A disease-impacted forest object A (surrounded by object neighbors B to H), versus (ii) a healthy forest object A (surrounded by object neighbors B to H). The color combinations were NIR-R-B.

(Mountain View, California, USA) high resolution imagery that were taken on July 29, 2007, close to the date when the KOMPSAT-2 data were acquired. A total of 200 points were collected following the random sampling strategy, with 50% of them used for calibration; while the remainder was used for validation. Finally, a classic confusion matrix and kappa statistic were reported for accuracy assessment.

3.2. Burn severity mapping

Burn severity mapping was carried out using a post-fire Landsat TM image and a physical simulation model proposed by De Santis et al. (2009). This model was developed linking the leaf-level PROSPECT (Jacquemoud, 1990) and canopy-level GeoSail (Verhoef and Bach, 2003) radiative transfer models, for the purpose of estimating various degrees of burn severity in Mediterranean ecosystems, directly applicable to forests of the Bug Sur region. Here, we did not choose empirical, statistical models, because such type of models using spectral indices including NDVI, dNDVI (differenced NDVI), NBR (Normalized Burn Ratio), or dNBR to estimate burn severity were found to have high variation in performance across geographical sites (Roy et al., 2006; De Santis and Chuvieco, 2007), possibly reducing the generalization capacity of our findings.

Model parameterization was conducted for PROSPECT and GeoSail, respectively. More specifically, the leaf-level PROSPECT model was parameterized to simulate spectra of two leaf types (green and brown), soil, dark charcoal, and light charcoal, which were further used as input for parameterizing the GeoSail model, making it possible to scale up from leaf to canopy level. The output of GeoSail was converted to a Look-up Table (LUT), comprised of 30 reference spectra (endmembers) corresponding to GeoCBI values from 0.0 to 3.0. These spectra were organized as a spectral library and, then, used as reference in the Spectral Angle Mapper supervised classification (Debba et al., 2005; Kruse et al., 1993) of the Landsat TM image. The result was a burn severity map, in which the corresponding GeoCBI value was assigned to each pixel of the post-fire image [see details of methodology in De Santis et al. (2009)]. Validation was performed comparing field-measured and simulated burn severity GeoCBI values.

3.3. Multiscale extraction of environmental factors

The environmental factors used in the study included landscape configuration, and topography. While there are a variety of factors affecting fire behavior and burn severity, our emphasis was the spatial patterns (i.e., landscape configuration) that were altered by sudden oak death emergence, as well as topographic factors that are crucial drivers of burn severity. Specifically, we employed landscape metrics that have demonstrated effectiveness in spatial pattern analysis (Turner, 1989; Wu et al., 2003; Coops et al., 2010). As pointed out by Godwin et al. (2015), many of these metrics have high correlations with each other, and no single metric is able to represent all aspects of the complex landscape structure. Here, we evaluated five representative metrics from the disease map: edge density (ED), contagion index (CONTAG), Shannon's diversity index (SHDI), and patch cohesion index (COHESION) [Table 2; refer to McGarigal (2014) for equations]. These metrics were chosen to represent four aspects of landscape patterns, including shape, dispersion/interspersion, diversity, and connectivity, respectively. They have been shown to be essential for various aspects of forest ecological function, such as analyzing the relationship between forest fragmentation and pine beetle outbreaks or wildfire in previous studies (e.g., Lee et al., 2009; Coops et al., 2010). The Fragstats package was employed in this study to calculate ED, CONTAG, SHDI and COHESION (McGarigal, 2014). The 8-neighbor rule was chosen for patch delineation treating both cardinal and diagonal pixels/cells as adjacent neighbors. This rule has been found to generate appropriate patches in previous studies (e.g., Linke et al., 2005; Richardson and Moskal, 2011; Godwin et al., 2015). Topographic factors included mean values of elevation, TMI (Topographic Moisture Index), slope, and aspect (Table 2; see data description in Section 2.3). In this study, we did not evaluate the impact of weather on burn severity, because such products were mainly developed at coarse resolutions and cannot meet our needs of assessing the multiscale effects.

All the factors were derived from 160 circular plots. Each of them was defined to have six sizes (diameter of 25, 50, 100, 150, 200, or 400 m) to account for the scale of impact from plot to landscape levels. That is, the center location of each plot was fixed across scales. For each plot, the change of scales was accomplished by changing the radius of the circular plot. Scale determination reflects the ecological characteristics of the Big Sur landscape. At the smallest plot scale (25 m), disease and fire impacts were observed to be relatively uniform and homogenous. Disease-impacted forests had greater than expected mortality among species that are often resilient to fire, a finding consistent with

Table 2
Descriptions of the extracted environmental factors at scales of 25, 50, 100, 150, 200, and 400 m.

Factor	Description
Landscape configuration:	
▪ ED	▪ Edge density
▪ CONTAG	▪ Contagion index
▪ SHDI	▪ Shannon's diversity index
▪ COHESION	▪ Patch cohesion index
Topography:	
▪ Elevation	▪ Mean elevation
▪ Slope	▪ Mean slope
▪ Aspect	▪ Mean aspect
▪ TMI	▪ Mean TMI (Topographic Moisture Index)

a previous stand-level study (Metz et al., 2013). Host species and topography started to show considerable variation at the scale of 100 m. At the 400 m plot scale, our study area revealed high spatial heterogeneity, which affected the spatial distributions of both disease and fire. To ensure a balanced representation of both healthy and disease-impacted forests, half of the plots were randomly extracted from the healthy forests using the land-cover classification map generated from Section 3.1, while the other half were from the disease-impacted forest class. At a large scale (e.g., 400 m), a plot could possibly contain both diseased and healthy trees. Here, we used a threshold of 75% to define each plot. That is, a plot was treated as diseased (or healthy) if >75% of the trees were affected by sudden oak death (or healthy). To ensure minimized spatial autocorrelation among the plots, we conducted a semivariogram analysis in ArcGIS environment (Esri, Redlands, California, USA), and found the effective distance of spatial autocorrelation was 600 m, which is smaller than the average distance between plots. We also set up a minimum distance value of 400 m between any two plot centers to avoid overlaps.

3.4. Statistical analyses

We developed generalized linear mixed models (GLMM) to link burn severity and the extracted environmental factors for healthy and disease-impacted forests, respectively. To test the scale effect, we also developed GLMMs at all the six scales. The identity link function was employed in GLMMs, because the observed burn severity followed log-normal distributions. Use of GLMMs allowed us to include random effects of plots within site, an approach recommended for ecological modeling when the data or experimental design has a nested hierarchy (Bolker et al., 2009). The models were developed at a 0.05 significance level using Akaike's information criterion (AIC) for determining the best model. To reduce multicollinearity, variance inflation factor (VIF) was calculated for all the predictors. By following a common rule of thumb, the explanatory variables were selected where VIFs were smaller than 10 in the final models. The development of all the mixed models were completed in SAS environment (Cary, North Carolina, USA).

4. Results

4.1. Disease mapping

The object-based classification selected five features (out of a total of 13) as input, including the maximum differential value, stand deviation for band 2 (blue), stand deviation for band 3 (near infrared), compactness, and length/width ratio. The results suggested the most accurate approach would employ all the three groups of features (spectral, texture, and geometry) in mapping *P. ramorum* caused tree mortality at the object level.

The object-based filtering algorithm resulted in a decrease of the spatial coverage of dead trees from 4.8% to 2.7% (Fig. 3). Although the absolute change in dead trees is a relatively small number, this was a 43.8% reduction in our dead tree estimate, which also represented a total area of 596 ha. The object-based filtering algorithm also resulted in increased estimates of bare ground and shrub/grass lands from 13.6% to 14.6%, and from 22.3% to 23.5%, respectively. Estimates of healthy forests amount and extent minimally changed likely because healthy forest objects were more heterogeneous. Compared to the bare ground and shrub/grass objects, healthy forests often had smaller object sizes. The accuracy of the final disease map (Fig. 3) was assessed with a confusion matrix and the derived Kappa statistic (Table 3). Specifically, the classification of healthy forest achieved the highest accuracies (user's accuracy: 95.24%; producer's accuracy: 86.96%). This was followed by the extraction of disease-impacted forest (user's accuracy: 80.00%; producer's accuracy: 85.71%), shrub/grass (user's accuracy: 84.00%; producer's accuracy: 84.00%), and bare ground (user's accuracy: 66.67%; producer's accuracy: 80.00%). The total accuracy and Kappa statistic were 85.00% and 0.85, respectively.

4.2. Burn severity mapping

The estimated burn severities from the employed radiative transfer models were found to overestimate burn effects. A comparison between estimated and field-measured GeoCBI values was conducted in healthy and diseased forests at three stages: 1) early stage where trees still retain their dead foliage (dried, brown leaves) and fine twigs; 2) middle stage where standing dead trees have lost fine crown fuels and the snags and large branches begin to fragment and fall; and 3) late stage where most trees have fallen and accumulated as ground fuels (Metz et al., 2013; Chen et al., 2015a). In healthy forests, the estimated burn severity and field plot data (ground truth data) showed a relatively high agreement ($r = 0.86$; RMSE = 0.53; Fig. 4). In contrast, *P. ramorum* caused tree mortality was found to introduce higher uncertainties in burn severity mapping. The early-stage infestation led to a relatively weak relationship ($r = 0.35$; RMSE = 0.73; Fig. 4); and the middle-stage showed a similar result ($r = 0.36$; RMSE = 0.56; Fig. 4). At the late-stage, the correlation between the two types of GeoCBI values increased ($r = 0.80$; RMSE = 0.51; Fig. 4) to the point where the burn severity model performance was similar to healthy forests. The burn severity was dominated by moderate ($1 \le$ GeoCBI ≤ 2) to severe ($2 \le$ GeoCBI ≤ 3) impacts for most of the study area, although notable areas of lower impact in canyon bottoms is apparent from the burn severity map (Fig. 5). Lower burn severity was also common in the northern part of the study region.

4.3. Linking burn severity and environmental factors in healthy and diseased forests

Environmental factors showed significant effects on burn severity but the effects of environment differed between healthy and disease-impacted forests. For healthy forests, the topographic variable elevation was a consistent factor driving burn severity in all the GLMMs (Table 4). Of the six tested scales, elevation was the sole significant explanatory variable at four scales with plot sizes ranging from 25, 50, 100 to 150 m. Landscape configuration variables did not demonstrate any significant effect on burn severity at the same spatial scales. With increasing observational scale to 200 and 400 m, the COHENSION variable representing connectivity of landscape patches also significantly influenced fire behavior, along with elevation (Table 4). We found a positive relationship between elevation and burn severity and a negative relationship between landscape connectivity and burn severity.

Disease infection altered the relationship between burn severity and its controlling environmental factors. In common with healthy forests, elevation was the sole explanatory variable of burn severity in disease-impacted forests at the 25 m scale. However, the landscape configuration variables had significant effects on burn severity at the scales of 50, 100, 150, and 200 m in disease-impacted forests (Table 5). Those variables included not only COHENSION, but also ED (shape of patches) and CONTAG (dispersion/interspersion of patches; Table 5).

5. Discussion

5.1. Assessment of disease mapping

Among the three groups of features (i.e., spectral, texture and geometry) needed to map *P. ramorum* caused tree mortality, maximum differential value calculated in a healthy forest was typically from near infrared (brightest) and green (darkest) bands. For the disease-impacted forests, the spectral reflectance in the near infrared band was reduced, sometimes reaching levels lower than the red or blue bands. Compared to an object classified as a healthy forest, a disease-impacted forest object typically had a smaller maximum differential value; but the

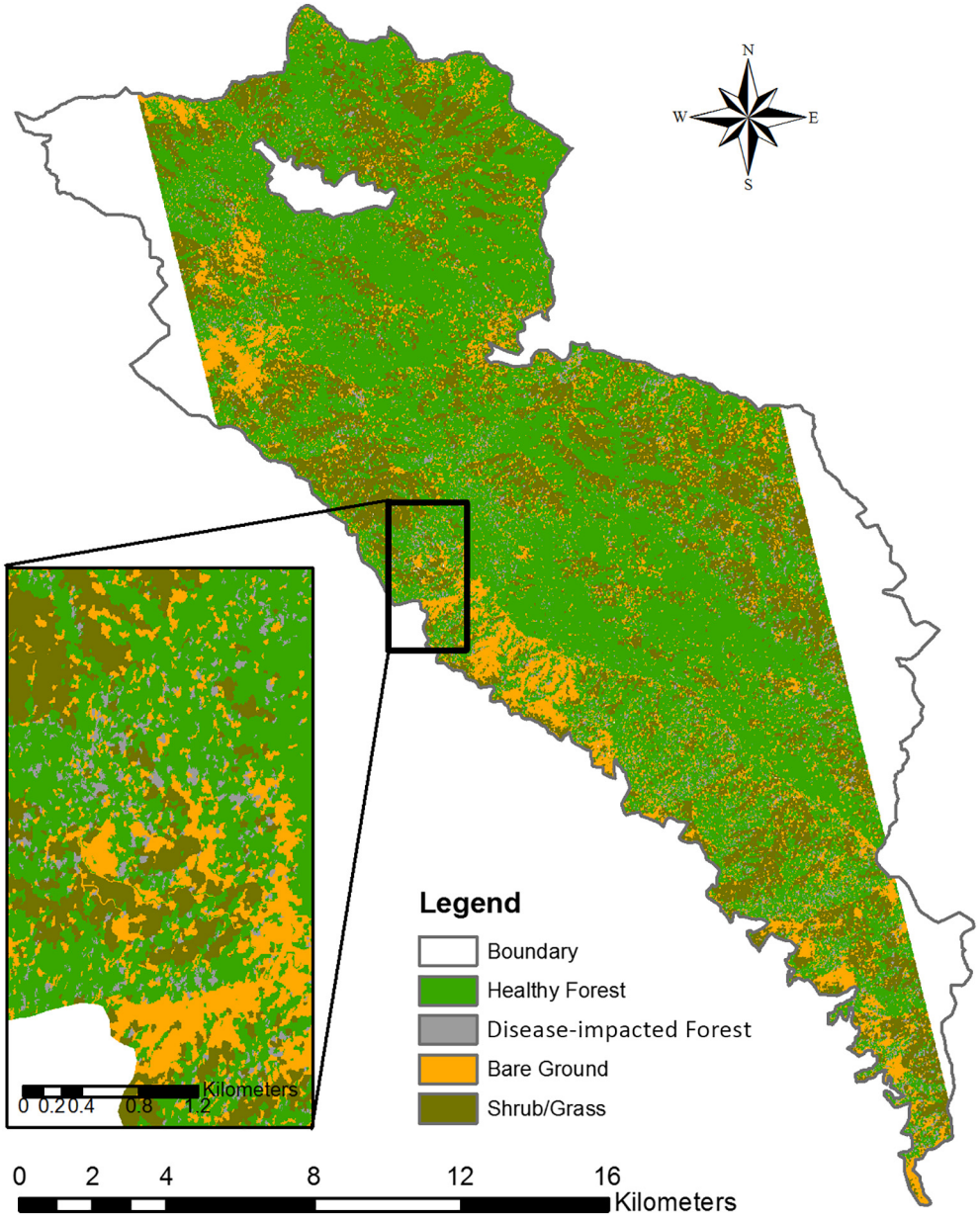

Fig. 3. Final disease map generated using object-based classification and object-based filtering.

range of this value often overlapped with that of a shrub/grass object. The texture features calculated from bands 2 and 3 helped differentiate the majority of forest objects (high variation) from the bare ground objects (low variation). Additionally, shrub/grass objects were relatively homogenous making them distinguishable from the forest objects. Complex sun-surface-sensor geometry can exert a high impact on the shape of image-objects in object-based image analysis (Chen et al., 2012b), while variation in tree 3D structure can further complicate forest object shape. The serrated edges of forest patches were found to be more irregular than those of non-forest objects, which resulted in low levels of compactness and higher length/width ratios.

Ideally, an image-object is internally homogenous representing one single land-cover class. However, Fig. 2 shows that multiple ground features (e.g., vegetation and bare ground) may be grouped into a single

Table 3
Confusion matrix and kappa statistic of the final disease mapping result.

User class	Reference class					
	Healthy forest	Disease-impacted forest	Bare ground	Shrub/grass	Total	User's accuracy (%)
Healthy forest	40	1	0	1	42	95.24
Disease-impacted forest	1	12	0	2	15	80.00
Bare ground	4	1	12	1	18	66.67
Shrub/grass	1	0	3	21	25	84.00
Total	46	14	15	25	100	
Producer's accuracy (%)	86.96	85.71	80.00	84.00		

Overall accuracy = 85.00%; Kappa statistic = 0.85.

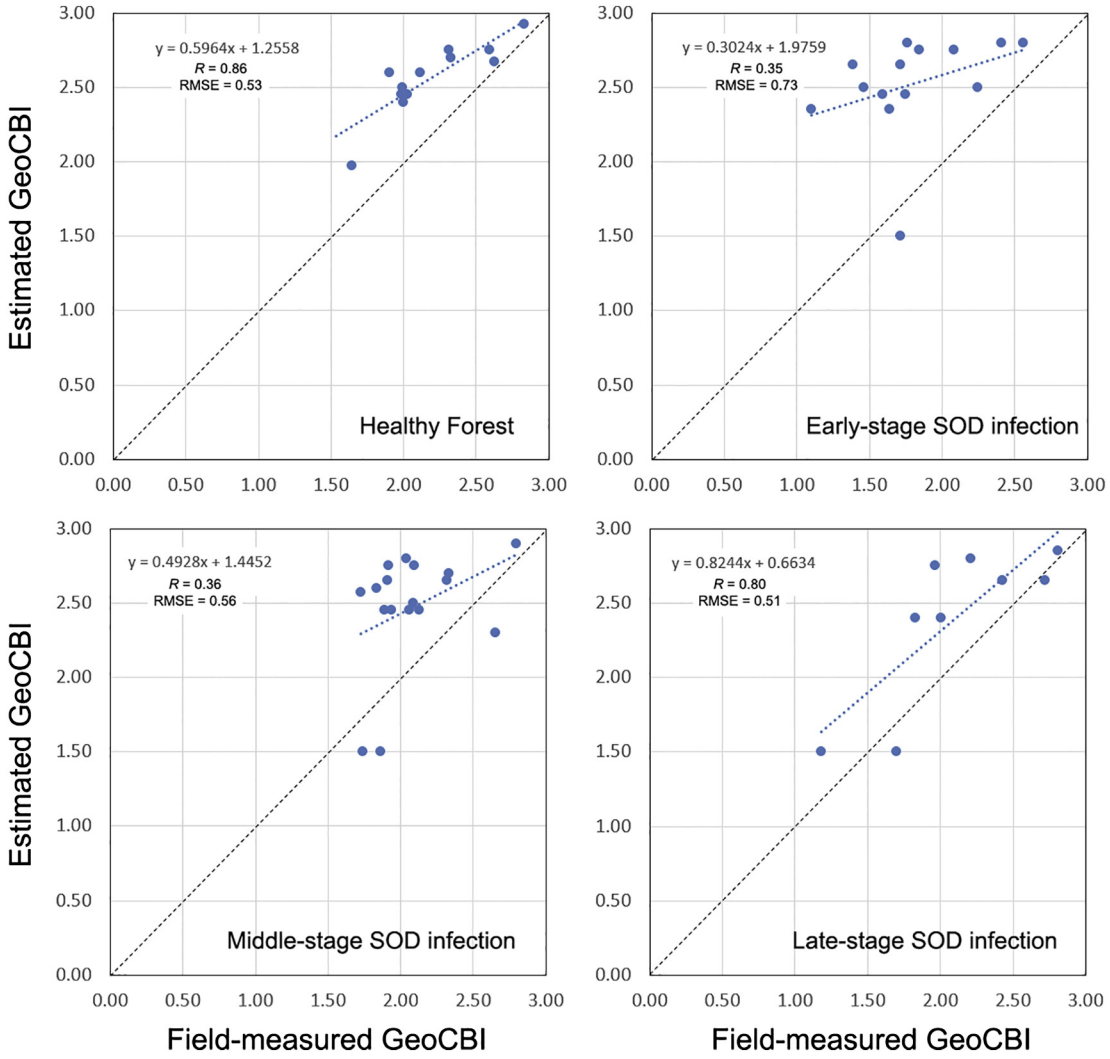

Fig. 4. Comparisons between field-measured GeoCBI and estimated GeoCBI across four types of forests: healthy, and early-, middle-, and late-stage sudden oak death progression.

object. This phenomenon is most frequent and potentially problematic in the transitional zones where the defined scale (used in segmentation) was too coarse to extract these features individually. It should be noted that the 'best scale' did not exist in our case study because it may vary from one transitional zone to another and depend on the landscape characteristics, including variation in fragmentation levels. Although misclassification is present in our final model products, object-based filtering increased accuracy of disease mapping over typical object-based classification, which was hampered by overestimation of infested trees (Fig. 3). It should also be noted that the remote detection of disease-caused tree damage was biased to certain stages where infected trees still showed dried foliage and/or branches. Disease or insect caused mortality remains challenging to detect with regular multispectral sensors (such as Landsat) when trees retain green pigment or at the late stage when material has been transferred to the forest floor but understory vegetation or regeneration is present (Chen and Meentemeyer, 2016).

The spatial distribution of disease-impacted forests in the classification map (Fig. 4) indicated that tree mortality mostly occurred on the western, coastal portion of the region. A previous study that mapped *P. ramorum* caused tree mortality up to 2005 in Big Sur, found similar spatial patterns and their results revealed that most of the host vegetation was located in the same portion of the landscape that contained the majority (63%) of dead trees (Meentemeyer et al., 2008). Although the data used by Meentemeyer et al. (2008) were two years prior to our data acquisition and the disease may have developed during this period, the spatial patterns of disease impacts remained similar to those predicted by spatial spread models as well as continued field plot resurveys (Meentemeyer et al., 2011; Metz et al., 2012). The change reflects the strong influence of climate and host distribution on sudden oak death spread and impacts.

5.2. Assessment of burn severity mapping

Our results clearly showed the challenges of estimating spatial patterns of burn severity in *P. ramorum* affected forests. At the early and middle infestation stages, the burn severity model that performed relatively well in healthy forests had inferior performance for these disease stages (Fig. 4). Dead tree crowns have lower foliage water content relative to healthy trees (Kuljian and Varner, 2010) and it was possible that the spectral reflectance from these crowns was similar to those affected by the fire. The high spectral similarity may have confused the PROSPECT and GeoSail models, which treated a portion of the diseased trees as affected by fire. Using land surface temperature derived from the Landsat thermal band(s) could be a potential solution to improve the accuracy of burn severity mapping (Quintano et al., 2017). In addition, as suggested by Chen et al. (2015b), high-spectral resolution sensors (e.g., MASTER) with mid- and thermal-infrared channels are more sensitive to the spectral variation caused by disease and fire. By complementing these data sources with Landsat, it may be possible to

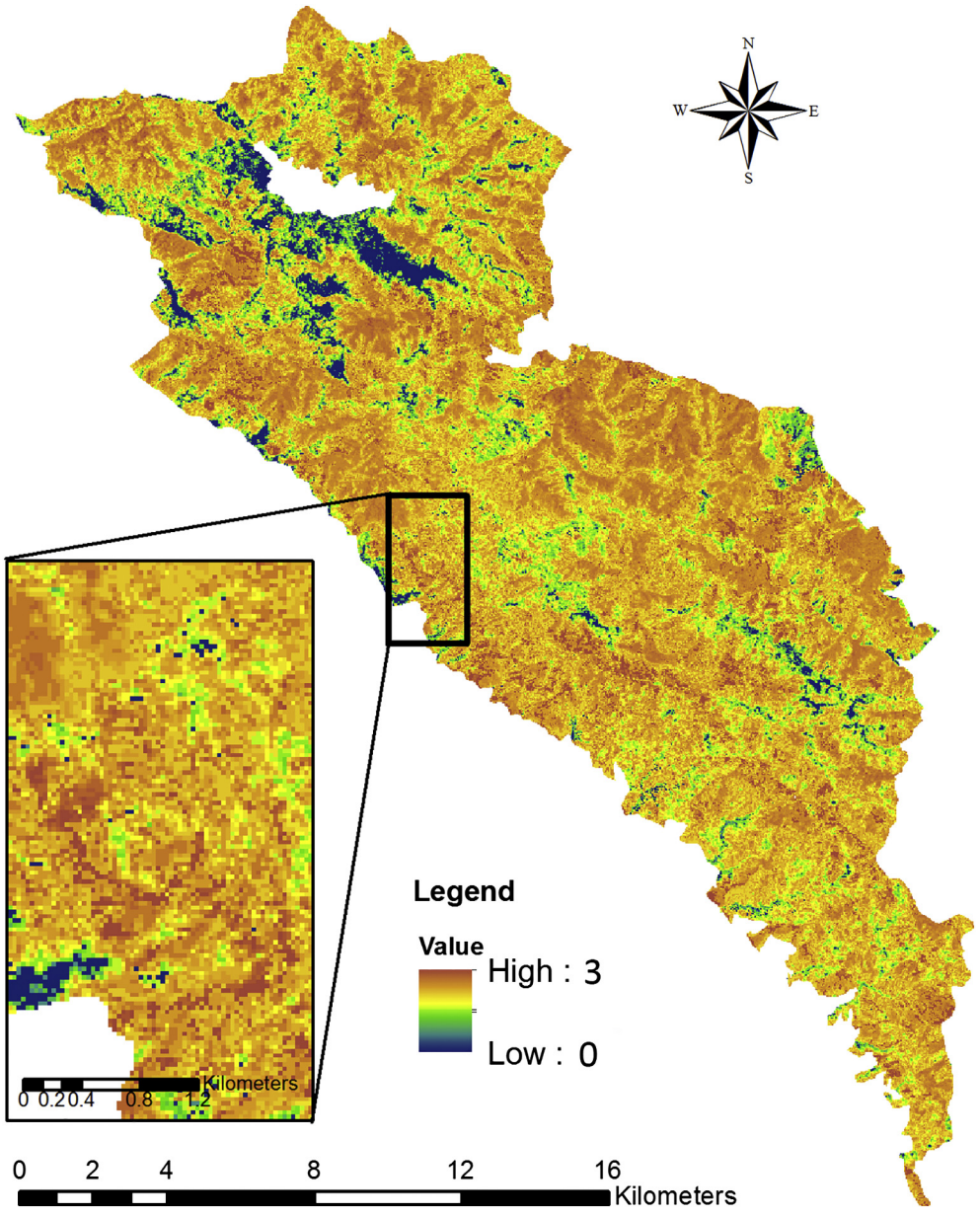

Fig. 5. Burn severity map of the study area.

Table 4
Estimates for predictors of the six evaluated scales, with results obtained by generalized linear mixed models in healthy forests.

Scale	Predictor	Estimate	Standard error	*t* Value
25 m	Intercept	1.0094	0.1958	5.16***
	Elevation	0.0001	0.0000	3.08**
50 m	Intercept	1.1182	0.2405	4.63***
	Elevation	0.0001	0.0000	3.12**
100 m	Intercept	0.8784	0.2500	3.51***
	Elevation	0.0003	0.0000	4.10***
150 m	Intercept	9.7171	5.7442	1.69
	Elevation	0.0003	0.0001	4.15***
200 m	Intercept	12.2343	5.2078	2.35*
	Elevation	0.0003	0.0001	4.15***
	COHESION	−0.1142	0.0526	−2.17***
400 m	Intercept	33.7411	7.5244	4.48***
	Elevation	0.0003	0.0001	5.42***
	COHESION	−0.3291	0.0760	−4.33***

* $p < 0.05$.
** $p < 0.01$.
*** $p < 0.001$.

achieve a higher accuracy in burn severity mapping. However, high-spectral resolution sensors are typically available on airborne platforms, which complicates their acquisition. We also found that the performance of the simulation model was greater for the later stage of disease progression where fallen trees often created canopy gaps. The accumulation of ground fuels in these late-stage disease conditions has been shown to be associated with greater soil burn severity and fire-caused tree mortality. These patterns suggest the ecological interactions between fire and disease are also dependent on the timing of fire given that sudden oak death creates both spatially and temporally heterogeneous fuel conditions (Metz et al., 2013; Cobb et al., 2016). Various stages of disease progression introduced different levels of uncertainties in remote detection and while such uncertainties were unavoidable, the burn severity mapping result met our accuracy criteria of RMSE <25% of the total range of index for burn severity applications (De Santis and Chuvieco, 2007). In our case, the maximum RMSE level is 0.75, which our models never exceeded. We are also aware of the time lag effect in our image and field data collection, which were two months after fire containment. This was mainly due to safety considerations and

Table 5
Estimates for predictors of the six evaluated scales, with results obtained by generalized linear mixed models in disease-impacted forests.

Scale	Predictor	Estimate	Standard error	*t* Value
25 m	Intercept	5.3616	0.1629	32.92***
	Elevation	0.0002	0.0000	3.12**
50 m	Intercept	0.5524	0.1830	3.02**
	Elevation	0.0001	0.0000	3.14**
	ED	0.0001	0.0000	2.59*
100 m	Intercept	8.1406	2.7837	2.92**
	Elevation	0.0001	0.0000	3.12**
	COHESION	−0.0773	0.0278	−2.78**
150 m	Intercept	12.7534	3.1074	4.10***
	Elevation	0.0002	0.0001	3.15**
	CONTAG	0.0027	0.0009	2.88**
	COHESION	−0.1237	0.0312	−3.97***
200 m	Intercept	0.8451	0.2454	3.44***
	Elevation	0.0001	0.0001	2.40*
	ED	0.0001	0.0000	2.62*
400 m	Intercept	4.2840	4.9250	0.87
	Elevation	0.0001	0.0001	2.44*

* $p < 0.05$.
** $p < 0.01$.
*** $p < 0.001$.

logistical limitations in field campaign. We recognize that this effect could possibly change the estimation of burn severity in some areas, hence affecting our conclusions. However, Landsat and field data were acquired in the similar time window, which minimized the impact of this time lag effect on remote sensing modeling.

5.3. Effect of plant disease on forest burn severity

Both types of GLMMs developed in healthy and diseased forests demonstrated the importance of elevation on burn severity during the basin fire. In our study area, the modeling results indicated burn severity was greater in forests at higher elevations (Table 4; Table 5). This pattern is also revealed by higher burn severities along ridgetops in the study region (Fig. 5). Elevation-burn severity patterns were consistent across spatial scales and disease conditions. Environmental controls of burn severity that reflect landscape configuration were found to vary between healthy and disease impacted forests. In healthy forests, the connectivity of landscape patches (i.e., COHESION) became a significant contribution to burn severity at the scale of 200 m, where tree species became more heterogeneous and land cover types would often include tree, shrub/grass and bare ground. Smaller COHESION values suggested more shrub/grass patches in healthy forest stands. Those patches were found with higher burn severity. Diseased forests showed a higher level of heterogeneity even at smaller scales. As noted by Davidson et al. (2005), sudden oak death typically demonstrates non-random, highly-localized distributions due to variation in host distribution and mortality rates of dead trees (see also Cobb et al., 2012; Metz et al., 2012). Disease increased landscape heterogeneity in the mixed oak and redwood-tanoak forest types where *P. ramorum* host densities are also greatest. Our burn severity model is consistent with this pattern in that landscape configuration had significant impacts at the small scale of 50 m. We also found that burn severity in disease-impacted forests was influenced by a wider range of factors related to landscape configuration including dispersion and patch shape. This pattern suggests disease-caused fuels accumulation either in the canopy (early and mid stage) or surface (later stage) may have influenced burn severity in nearby vegetation including ecosystems where *P. ramorum* does not establish or causes mortality.

Lee et al. (2009) argued that a more heterogeneous landscape structure tends to reduce fire risk and burn severity in a pine dominated forest. In contrast, our study revealed a modification of these relationships with disease, likely through changes in fuel levels and distribution across the landscape. In Big Sur, a landscape comprising less connected patches (smaller COHENSION values) and higher patch shape complexity (larger ED values) was more likely to experience greater burn severity. These patterns are consistent with fuels accumulation in diseased areas resulting in impacts to adjacent forests, either through more frequent high fuels locations (higher CONTAG values) or greater shared borders between areas of higher fuels accumulation and non-disease impacted forests (higher ED values). In a case study of forest fire in Catalonia, Spain, González et al. (2005) compared two types of metrics in forest fire risk modeling, including the non-spatial mean fire resistance of the landscape, and the spatial landscape configuration. Among all the tested metrics, the non-spatial metric was found to be the most important factor affecting fire behavior. This finding is a useful contrast to our study region given that both studies share a similar Mediterranean climate. Although sudden oak death increased landscape heterogeneity, it also reduced the mean fire resistance of the landscape likely through a well-documented increase in fuel loads in diseased forests (Kuljian and Varner, 2010; Cobb et al., 2012; Metz et al., 2013; Cobb et al., 2016). Our results indicated that for sudden oak death and the basin fire, reduced fire resistance may have played a more important role than the increased spatial heterogeneity in affecting burn severity.

The extent to which these findings are common to other forest types is uncertain given the general lack of studies examining outbreak-fire interactions (Simard et al., 2011; Metz et al., 2013). The few data-driven examples suggest these relationships are dependent on biophysical factors that influence fire dynamics across or between regions. For example, in a study of lodgepole pine (*Pinus contorta*) impacted by bark beetle, the probability of transitions from ground fire to canopy fire decreased with the transfer of dead foliage from the canopy to the soil surface (Simard et al., 2011). The transition of fine fuels from the canopy of *P. ramorum*-killed trees to the soil surface is also likely to reduce the potential for crown fire in these systems (Kuljian and Varner, 2010), although with the additional impacts of increased soil impacts and mortality of trees that otherwise could be expected to survive fire (Metz et al., 2013; Cobb et al., 2016). We caution against applying our results to unstudied outbreak-fire systems without evidence to support an expected direction or magnitude of impact. At the same time, our results strongly suggest these interactions are worth evaluating in a greater range of forest types.

6. Conclusions

There is increasing evidence that wildfire, and pathogen or insect outbreak can occur simultaneously in forest ecosystems and that the resulting tree mortality can have complex and sometimes positive effects on burn severity. During the 2008 Basin Fire, landscape configuration and topography were important influences on burn severity. Baseline maps of burn severity and disease-caused mortality derived from Landsat and high-resolution KOMPSAT-2 satellite used a new object-based filter, which reduced overestimation of diseased forests. Sudden oak death altered surface fuel loads and landscape heterogeneity. Although these changes could have opposite effects on burn severity, our findings indicated that the increased fuel loads increased burn severity in adjacent forests. While derived from a single fire and disease outbreak, our results imply that landscape-level disease conditions could influence fire impacts at similar spatial scales for other forest types and disturbances and that landscape-level investigations may be needed to detect disturbance interactions in some ecosystems. Fire is a critically important landscape structuring force in many forests suggesting greater attention to understanding fire interactions with other landscape-level disturbances such as insect or disease outbreak can improve prediction of impacts as well as management responses. Understanding disturbance interactions allows us to better maintain a “safe operating space” for ecosystem recovery (Johnstone et al., 2016).

Acknowledgement

This research was supported by the National Science Foundation (EF-0622770) as part of the joint NSF-NIH Ecology and Evolution of Infectious Disease program, the North Carolina Space Grant, and the University of North Carolina at Charlotte CLAS Junior Faculty Development Award. The authors also gratefully acknowledge financial support from the USDA Forest Service – Pacific Southwest Research Station, and the Gordon & Betty Moore Foundation. We thank numerous contributors who provided vital field and laboratory support, including K. Aram, M. Beh, A. Brauer, M. Chan, C, DeLong, W. Dillon, K. Frangioso, A. Hohl, H. Mehl, A. Oguchi, E. Paddock, K. Pietrzak, M. Vaclavikova, J. Vieregge, L. Waks and A. Wickland.

References

Asner, G.P., 2013. Geography of forest disturbance. Proc. Natl. Acad. Sci. 110, 3711–3712.
ASTER GDEM Validation Team, 2011. ASTER Global Digital Elevation Model Version 2 – Summary of Validation Results. Available online. http://www.jspacesystems.or.jp/ersdac/GDEM/ver2Validation/Summary_GDEM2_validation_report_final.pdf.
Balbi, J.H., Morandini, F., Silvani, X., Filippi, J.B., Rinieri, F., 2009. A physical model for wildland fires. Combust. Flame 156, 2217–2230.
Beven, K.J., Kirkby, M.J., 1979. A physically based, variable contributing area model of basin hydrology. Hydrol. Sci. Bull. 24, 43–69.
Bolker, B.M., Brooks, M.E., Clark, C.J., Geange, S.W., Poulsen, J.R., Stevens, M.H.H., White, J.S.S., 2009. Generalized linear mixed models: a practical guide for ecology and evolution. Trends Ecol. Evol. 24, 127–135.
Boyd, I.L., Freer-Smith, P.H., Gilligan, C.A., Godfray, H.C.J., 2013. The consequence of tree pests and diseases for ecosystem services. Science 342, 1235773.
Chavez Jr, P.S., 1996. Image-based atmospheric corrections—revisited and improved. Photogramm. Eng. Remote. Sens. 62, 1025–1036.
Chen, G., Meentemeyer, R.K., 2016. Remote sensing of forest damage by diseases and insects. In: Weng, Q. (Ed.), Remote Sensing for Sustainability. CRC Press, Taylor & Francis Group, Boca Raton, Florida, pp. 145–162.
Chen, G., Hay, G.J., Castilla, G., St-Onge, B., 2011. A multiscale geographic object-based image analysis to estimate lidar-measured forest canopy height using Quickbird imagery. Int. J. Geogr. Inf. Sci. 25, 877–893.
Chen, G., Hay, G.J., St-Onge, B., 2012a. A GEOBIA framework to estimate forest parameters from lidar transects, Quickbird imagery and machine learning: a case study in Quebec, Canada. Int. J. Appl. Earth Obs. Geoinf. 15, 28–37.
Chen, G., Hay, G.J., Carvalho, L.M.T., Wulder, M.A., 2012b. Object-based change detection. Int. J. Remote Sens. 33, 4434–4457.
Chen, G., Metz, M.R., Rizzo, D.M., Dillon, W.W., Meentemeyer, R.K., 2015a. Object-based assessment of burn severity in diseased forests using high-spatial and high-spectral resolution MASTER airborne imagery. ISPRS J. Photogramm. Remote Sens. 102, 38–47.
Chen, G., Metz, M.R., Rizzo, D.M., Meentemeyer, R.K., 2015b. Mapping burn severity in a disease-impacted forest landscape using Landsat and MASTER imagery. Int. J. Appl. Earth Obs. Geoinf. 40, 91–99.
Chuvieco, E., 1999. Measuring changes in landscape pattern from satellite images: short-term effects of fire on spatial diversity. Int. J. Remote Sens. 22, 2331–2346.
Cobb, R.C., Filipe, J.A.N., Meentemeyer, R.K., Gilligan, C.A., Rizzo, D.M., 2012. Ecosystem transformation by emerging infectious forest disease: loss of large tanoak from California forests. J. Ecol. 100, 712–722.
Cobb, R.C., Meentemeyer, R.K., Rizzo, D.M., 2016. Interactive impacts of fire and disease on soil chemistry and carbon. Oecologia 182, 265–276.
Coops, N.C., Gillanders, S.N., Wulder, M.A., Gergel, S.E., Nelson, T., Goodwin, N.R., 2010. Assessing changes in forest fragmentation following infestation using time series Landsat imagery. For. Ecol. Manag. 259, 2355–2365.
Davidson, J.M., Wickland, A.C., Patterson, H.A., Falk, K.R., Rizzo, D.M., 2005. Transmission of *Phytophthora ramorum* in mixed–evergreen forest in California. Phytopathology 95, 587–596.
Davis, F.W., Borchert, M.I., Flint, A., Meentemeyer, R.K., Rizzo, D.M., 2010. Pre-impact forest composition and ongoing tree mortality associated with sudden oak death disease in the Big Sur region, California. For. Ecol. Manag. 259, 2342–2354.
De Santis, A., Chuvieco, E., 2007. Burn severity estimation from remotely sensed data: performance of simulation versus empirical models. Remote Sens. Environ. 108, 422–435.
De Santis, A., Chuvieco, E., 2009. GeoCBI: a modified version of the Composite Burn Index for the initial assessment of the short-term burn severity from remotely sensed data. Remote Sens. Environ. 113, 554–562.
De Santis, A., Chuvieco, E., Vaughan, P.J., 2009. Short-term assessment of burn severity using the inversion of PROSPECT and GeoSail models. Remote Sens. Environ. 113, 126–136.
Debba, P., van Ruitenbeek, F.J.A., van der Meer, F.D., Carranza, J.M., Stein, A., 2005. Optimal field sampling for targeting minerals using hyperspectral data. Remote Sens. Environ. 99, 373–386.
Epting, J., Verbyla, D., Sorbel, B., 2005. Evaluation of remotely sensed indices for assessing burn severity in interior Alaska using Landsat TM and ETM +. Remote Sens. Environ. 96, 328–339.
Godwin, C., Chen, G., Singh, K.K., 2015. The impact of urban residential development patterns on forest carbon density: an integration of LiDAR, aerial photography and field mensuration. Landsc. Urban Plan. 136, 97–109.
González, J.R., Palahí, M., Pukkala, T., 2005. Integrating fire risk considerations in forest management planning in Spain – a landscape level perspective. Landsc. Ecol. 20, 957–970.
Harvey, B.J., Donato, D.C., Romme, W.H., Turner, M.G., 2013. Influence of recent bark beetle outbreak on fire severity and postfire tree regeneration in montane Douglas-fir forests. Ecology 94, 2475–2486.
Hicke, J.a., Johnson, M.C., Hayes, J.L., Preisler, H.K., 2012. Effects of bark beetle-caused tree mortality on wildfire. For. Ecol. Manag. 271, 81–90.
Jacquemoud, S., 1990. PROSPECT: a model to leaf optical properties spectra. Remote Sens. Environ. 34, 74–91.
Johnstone, J.F., Allen, C.D., Franklin, J.F., et al., 2016. Changing disturbance regimes, ecological memory, and forest resilience. Front. Ecol. Environ. 14, 369–378.
Jolly, W.M., Parsons, R., Varner, J.M., Butler, B.W., Ryan, K.C., Gucker, C.L., 2012. Do mountain pine beetle outbreaks change the probability of active crown fire in lodgepole pine forests? Comment. Ecology 93, 941–946.
Keeley, J.E., 2009. Fire intensity, fire severity and burn severity: a brief review and suggested usage. Int. J. Wildland Fire 18, 116–126.
Kelly, M., Meentemeyer, R.K., 2002. Landscape dynamics of the spread of sudden oak death. Photogramm. Eng. Remote. Sens. 68, 1001–1009.
Key, C., Benson, N., 2005. Landscape assessment: ground measure of severity; the Composite Burn Index, and remote sensing of severity, the Normalized Burn Index. In: Lutes, D., Keane, R., Caratti, J., Key, C., Benson, N., Sutherland, S., Gangi, L. (Eds.), FIREMON: Fire Effects Monitoring and Inventory System. Rocky Mountains Research Station, USDA Forest Service, Fort Collins, CO, USA, pp. 1–51.
Kokaly, R.F., Rockwell, B.W., Haire, S.L., King, T.V.V., 2007. Characterization of post-fire surface cover, soils, and burn severity at the Cerro Grande Fire, New Mexico, using hyperspectral and multispectral remote sensing. Remote Sens. Environ. 106, 305–325.
Kruse, F.A., Lefkoff, A.B., Boardman, J.B., Heidebrecht, K.B., Shapiro, A.T., Barloon, P.J., et al., 1993. The spectral image processing (SIPS)—interactive visualization of imaging spectrometer data. Remote Sens. Environ. 44, 145–163.
Kuljian, H., Varner, J.M., 2010. The effects of sudden oak death on foliar moisture content and crown fire potential in tanoak. For. Ecol. Manag. 259, 2103–2110.
Lee, S.-W., Lee, M.-B., Lee, Y.-G., Won, M.-S., Kim, J.-J., Hong, S., 2009. Relationship between landscape structure and burn severity at the landscape and class levels in Samchuck, South Korea. For. Ecol. Manag. 258, 1594–1604.
Lentile, L.B., Holden, Z.A., Smith, A.M.S., Falkowski, M.J., Hudak, A.T., Morgan, P., Lewis, A.A., Gessler, P.E., Benson, N.C., 2006. Remote sensing techniques to assess active fire characteristics and post-fire effects. Int. J. Wildland Fire 15, 319–345.
Levin, S.A., 1992. The problem of pattern and scale in ecology. Ecology 73, 1943–1967.
Linke, J., Franklin, S.E., Huettmann, F., Stenhouse, G.B., 2005. Seismic cutlines, changing landscape metrics and grizzly bear landscape use in Alberta. Landsc. Ecol. 20, 811–826.
Liu, D., Kelly, M., Gong, P., 2006. A spatial–temporal approach to monitoring forest disease spread using multi-temporal high spatial resolution imagery. Remote Sens. Environ. 101, 167–180.
Lloret, F., Calvo, E., Pons, X., Díaz-Delgado, R., 2002. Wildfires and landscape patterns in the eastern Iberian Peninsula. Landsc. Ecol. 17, 745–759.
McGarigal, K., 2014. FRAGSTATS Help. University of Massachusetts, Amherst, MA (209 pp.).
Meentemeyer, R.K., Rank, N.E., Shoemaker, D., Oneal, C., Wickland, A.C., Frangioso, K.M., Rizzo, D.M., 2008. Impact of sudden oak death on tree mortality in the Big Sur ecoregion of California. Biol. Invasions 10, 1243–1255.
Meentemeyer, R.K., Cunniffe, N.J., Cook, A.R., Filipe, J.A.N., Hunter, R.D., Rizzo, D.M., Gilligan, C.A., 2011. Epidemiological modeling of invasion in heterogeneous landscapes: spread of sudden oak death in California (1990–2030). Ecosphere 2, art17.
Metz, M.R., Frangioso, K.M., Meentemeyer, R.K., Rizzo, D.M., 2011. Interacting disturbances: wildfire severity affected by stage of forest disease invasion. Ecol. Appl. 21, 313–320.
Metz, M.R., Frangioso, K.M., Wickland, A.C., Meentemeyer, R.K., Rizzo, D.M., 2012. An emergent disease causes directional changes in forest species composition in coastal California. Ecosphere 3, art86.
Metz, M.R., Varner, J.M., Frangioso, K.M., Meentemeyer, R.K., Rizzo, D.M., 2013. Unexpected redwood mortality from synergies between wildfire and an emerging infectious disease. Ecology 94, 2152–2159.
Quintano, C., Fernández-Manso, A., Roberts, D.A., 2013. Multiple Endmember Spectral Mixture Analysis (MESMA) to map burn severity levels from Landsat images in Mediterranean countries. Remote Sens. Environ. 136, 76–88.
Quintano, C., Fernandez-Manso, A., Roberts, D.A., 2017. Burn severity mapping from Landsat MESMA fraction images and Land Surface Temperature. Remote Sens. Environ. 190, 83–95.
Richardson, J.J., Moskal, L.M., 2011. Strengths and limitations of assessing forest density and spatial configuration with aerial LiDAR. Remote Sens. Environ. 115, 2640–2651.
Rizzo, D.M., Garbelotto, M., Hansen, E.M., 2005. *Phytophthora ramorum*: integrative research and management of an emerging pathogen in California and Oregon forests. Annu. Rev. Phytopathol. 43, 309–335.
Rogan, J., Franklin, J., 2001. Mapping wildfire burn severity in Southern California forests and shrublands using enhanced thematic mapper imagery. Geocarto Int. 16, 91–106.
Roy, D.P., Boschetti, L., Trigg, S.N., 2006. Remote sensing of fire severity: assessing the performance of the normalized burn ratio. IEEE Geosci. Remote Sens. Lett. 3, 112–116.
Simard, M., Romme, W.H., Griffin, J.M., Turner, M.G., 2011. Do mountain pine beetle outbreaks change the probability of active crown fire in lodgepole pine forests? Ecol. Monogr. 81, 3–24.

Stephens, S.L., Agee, J.K., Fulé, P.Z., North, M.P., Romme, W.H., Swetnam, T.W., Turner, M.G., 2013. Land use. Managing forests and fire in changing climates. Science 342, 41–42.
Trimble, 2012. eCognition Developer 8.7.2 Reference Book. Definiens AG, Munich, Germany (440 pp.).
Turner, M.G., 1989. Landscape ecology: the effect of pattern on process. Annu. Rev. Ecol. Evol. Syst. 20, 171–197.
Turner, M.G., Romme, W.H., 1994. Landscape dynamics in crown fire ecosystems. Landsc. Ecol. 9, 59–77.
USDA Forest Service, 2008. Executive Summary: Basin Complex Fire/Indians Fire BAER Initial Assessment (16 pp.).
USGS, 2016. Landsat Collections. Available online. http://landsat.usgs.gov/landsatcollections.php.
van Wagtendonk, J.W., Root, R.R., Key, C.H., 2004. Comparison of AVIRIS and Landsat ETM+ detection capabilities for burn severity. Remote Sens. Environ. 92, 397–408.
Verhoef, W., Bach, H., 2003. Simulation of hyperspectral and directional radiance images using coupled biophysical and atmospheric radiative transfer models. Remote Sens. Environ. 87, 23–41.
Welch, R., Ahlers, W., 1987. Merging multiresolution SPOT HRV and landsat TM data. Photogramm. Eng. Remote. Sens. 53, 301–303.
Wu, J., 2004. Effects of changing scale on landscape pattern analysis: scaling relations. Landsc. Ecol. 19, 125–138.
Wu, J., Shen, W., Sun, W., Tueller, P.T., 2003. Empirical patterns of the effects of changing scale on landscape metrics. Landsc. Ecol. 17, 761–782.
Wulder, M.A., Dymond, C.C., White, J.C., Leckie, D.G., Carroll, A.L., 2006. Surveying mountain pine beetle damage of forests: a review of remote sensing opportunities. For. Ecol. Manag. 221, 27–41.
Xiao, X., Boles, S., Liu, J., Zhuang, D., Liu, M., 2002. Characterization of forest types in Northeastern China, using multi-temporal SPOT-4 VEGETATION sensor data. Remote Sens. Environ. 82, 335–348.